Reconfigurable Design of mmWave Liquid-Crystal Frequency Selective Surface at Ka-Band

Hsi-Hsir Chou, *Senior Member, IEEE*, Guan-Jhou Ke, Cheng-Chung Lin, and Guo-Sheng Lin

***Abstract*—A reconfigurable design of frequency selective surface (FSS) using nematic liquid crystal (LC) materials is reported. The proposed LC-FSS resonates at Ka-band frequencies to provide a bandpass nature. The frequency selection was achieved by altering the dielectric anisotropy of LC materials. This study used a low-cost Merck-E7 LC material with dielectric tunability of nearly 0.45 to study the resonance characteristics. Full-wave simulations have achieved a frequency tunability range of 5.06%. An LC-FSS prototype of 7 cm × 7 cm in size was fabricated for experimental evaluation, consisting of 25 × 25 unit cells. The measurement results show that a maximum frequency tunability close to 4.8% has been achieved for a normally incident illumination of electromagnetic waves. Moreover, the maximum frequency deviations were only 4.73% and 4.94% with/without a bias voltage to shift the center frequency. These experimental results have precisely verified the numerical simulations despite the frequency deviations resulting from the fabrication tolerances.**

***Index Terms*—Bandpass filter, frequency selective surface (FSS), liquid crystals (LCs), polarization-insensitivity.**

I. Introduction

THE frequency selective surface (FSS) has been intensively investigated for decades for many practical applications. Military applications can be used as radomes to protect antennas and electromagnetic (EM) wave absorbers in stealth technologies. In communications, they can also reduce EM interferences and shield the transmitters' and receivers' electronic devices against the unwanted EM waves [1]–[7]. In contrast to the conventional design of passive FSS structure, the trend tends to produce reconfigurability for FSSs. Several useful technologies, such as using PIN diodes, varactor diodes, and microelectromechanical systems (MEMs), have been proposed to switch between different states of structural variations. However, severe limitations exist to prevent them from wide applications [8]–[10]. For example, the diode-based approaches suffer severe parasitic inductance and significant dielectric loss at high frequencies, limiting the applicable frequency ranges. Although the MEMS-based approaches can be used at higher operational frequencies beyond 100 GHz, it requires a complicated and costly process to fabricate. They cannot fulfill low cost, low power, and compact configuration in modern FSS applications. Moreover, the degree of reconfiguration is very low to produce a good performance. Other technology developments to achieve the reconfigurability for FSSs by integrating standard metasurface with phase-change materials, such as graphene [11], vanadium dioxide (VO2) [12], and liquid crystals (LCs) [13], have also been reported. However, most of the demonstrated works, such as using graphene [11] and vanadium dioxide (VO2) [12], were majority focused on the scope of terahertz frequencies.

On the other hand, LC materials attracted much attention for their flexible dielectric characteristics. The advantage of altering the equivalent dielectric permittivity by applying low voltages [13] to change the molecule orientations of LC materials makes them attractive to design reconfigurable FSSs. They can produce a wide range of tunable dielectric permittivity and result in a wide range of reconfigurable operational frequencies. In principle, the LC-based FSS (referred to as LC-FSS, hereafter) has no limitation of operating frequencies. The operations at beyond 100 GHz have been demonstrated in [13] and [14]. Several works of LC-FSS for the applications at lower frequency bands, including industrial scientific medical bands [15], S-band [16], and X-band [17], [18], have also been reported. However, most of them were investigated numerically. In particular, the LC-FSS for the millimeter-wave (mmWave) applications at Ka-band has rarely been investigated. Although there has been experimental works demonstrated recently [13], [18], the fabrication processes were majority based on glass substrates, which will require a very high process cost and the practical applications will also be limited. Moreover, the used LC materials were all customized and not commercially available.

Progressing from our previous works in [19] and [20], we further report the experimental investigation of a novel tunable bandpass LC-FSS utilizing the coupled method [21], [22] and low-cost LC materials. The LC materials are Merck-E7, which have been widely used for mass productions in display applications. The designed LC-FSS resonates at Ka-band between 30 and 31.6 GHz. The dielectric permittivity tunable range of the LC material is close to 0.45 [23] and results in a frequency tunability of 5.06%, as observed from numerical simulations.

Manuscript received 21 April 2022; revised 28 June 2022; accepted 19 July 2022. This work was supported in part by the National Chung-Shan Institute of Science and Technology, Taiwan, under Grant XD909025P400-CS and in part by MOST, Taiwan, under Grant MOST 110-2221-E-011-054. *(Corresponding author: Hsi-Hsir Chou.)*

Hsi-Hsir Chou and Guan-Jhou Ke are with the Department of Electronic and Computer Engineering, National Taiwan University of Science and Technology, Taipei 106, Taiwan (e-mail: hsi-hsir.chou@trinity.cantab.net; m10802310@mail.ntust.edu.tw).

Cheng-Chung Lin and Guo-Sheng Lin are with the Chemical Systems Research Division, National Chung-Shan Institute of Science and Technology, Taoyuan 32599, Taiwan (e-mail: dannycclin@gmail.com; gslinmark@gmail.com).

Color versions of one or more figures in this article are available at https://doi.org/10.1109/TEMC.2022.3193995.

Digital Object Identifier 10.1109/TEMC.2022.3193995

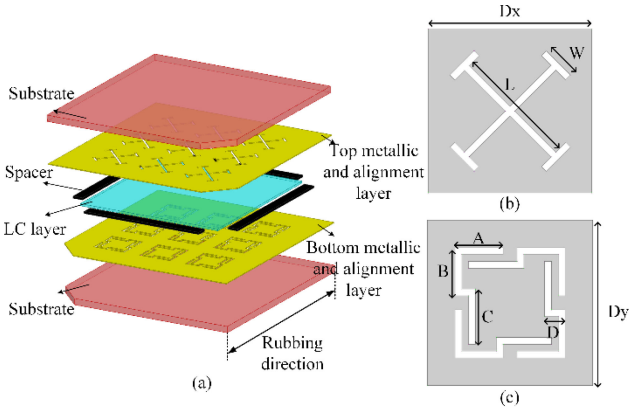

Fig. 1. Proposed LC-FSS. (a) Structure. (b) Jerusalem cross aperture on the top metallic layer and (c) a four-aperture slot pattern on the bottom metallic layer caption.

These simulation results have been further verified through an experimental LC-FSS prototype with a good agreement between the simulation and measurement results. The proposed work is the first experimental investigation for an LC-FSS resonating at Ka-band frequencies based on low-cost LC material and print circuit board (PCB) technology to the best of our knowledge. When using this LC-FSS as absorbers, it also offers better performance with a smaller thickness than conventional absorbers [24]–[29]. Moreover, depending on the configuration of LC materials, the proposed design can be applied to treat different polarization properties due to the symmetric patterns used on each metallic layer. Unlike the most traditional use of diode components (pin-diode) to create the reconfigurability of FSS-based absorbers, which have frequency band limitation, high loss, high cost, complicated system structure, and other shortcomings [30], [31], the development of the proposed work is not limited by the frequency band and can also be implemented by low-cost PCB substrates, thus providing an efficient approach for the direct mass production of a tunable LC-FSS for Ka-band applications. The rest of this article is organized as follows. Section II describes the fundamental architecture of the proposed LC-FSS. The full-wave performance simulations are analyzed in Section III. The experimental implementation and measurement results are reported in Section IV. Finally, Section V concludes this article.

II. Fundamental Architecture of LC-FSS

The proposed LC-FSS architecture is illustrated in Fig. 1, which conceptually consists of three planar dielectric substrate layers based on low-cost PCB technology. In particular, the intermediate layer at the middle is made of reconfigurable LC materials, whose dielectric properties of dielectric permittivity and loss tangent will be altered by controlling the applied bias voltages. This LC layer is sandwiched by two ordinary dielectric substrates of RO 4350 [32] with $\varepsilon_r = 3.66$ and $\tan\delta = 0.004$. The bottom and top surfaces of the sandwiching dielectric substrates facing the LC layer are coated with copper foils of 0.035 mm in each thickness. It is noted that there are two extremely thin alignment layers coated on the surfaces of these two copper foils by polyvinyl alcohol (PVA) films to accommodate the LC materials and adjust the proper molecule orientations. This ensures that the LC molecules between these two metallic layers are aligned uniformly along a pretilt angle.

The LC material's dielectric properties are appropriately altered by applying proper voltage between these two copper surfaces. In this case, the thickness of the LC layer is 100 μm, whereas RO 4350 dielectric substrates have equal thicknesses of 0.762 mm with an additional metal coating of 0.035 mm by copper foils. Two corners are trimmed out on the top and bottom substrates, respectively, on the adjacent corners to implement metal wires to apply the bias voltages easily on the top and bottom metal surfaces, respectively. In order to explore the frequency selection limitation, only two voltages states of 0 and 10 V are used to alter the dielectric properties. Since the Merck-E7 LC materials have the relative permittivity of 2.72 and 3.17, and the loss tangent of 0.05 and 0.033 [23], respectively, for the vertical and horizontal molecule arrangement to form the LC layer. At the 0-V state of the applying voltage, the LC substrate exhibits a dielectric permittivity of 2.72 and $\tan\delta = 0.05$. When the external voltage exceeds the threshold of bias voltage (10 V), the electronic field polarized in the vertical direction of these metallic layers will be uniformly produced to change the arrangement of the LC molecules. In this case, the dielectric permittivity and loss tangent of LC materials change to 3.17 and $\tan\delta = 0.033$. This mechanism well controls the dielectric constants of the LC layer. It will be shown later that one only needs few discrete voltages to produce a broad frequency bandwidth due to the bandwidth overlapping by the reflection coefficient curves.

The metal surfaces of the top and bottom dielectric substrates implement periodic FSS elements of different patterns to produce a spatial bandpass nature. In particular, each metallic layer was realized by a type of single-layer bandpass filter. In the single-layer spatial filter designs, the center operation frequencies were determined by the aperture lengths, which can be theoretically calculated in light of the approach provided from the literature [1], [2], [21], [22]. In the proposed work as illustrated in Fig. 1(b) and (c), the unit cell patterns on the top metallic layer were designed by 45° tilted Jerusalem cross aperture slots. On the other hand, four detoured aperture slots were created to form the unit cell patterns on the bottom metallic layer, which is a revised design extended from the conventional square pattern. In this configuration, arbitrary aperture slot length can be chosen without changing the size of the unit cell since it is well known from the literature [33] that the smaller the size of the unit cell (relative to wavelength), the better the angular stability.

The LC materials are inserted in the middle region, as illustrated in Fig. 1(a), by the light blue color. The black strips around it are boundary spacers to form a cavity for the LC materials. The top and bottom metallic layers were also designed to serve as the bias layers to drive the LC layer by applying electric voltages. Therefore, slot-type footprints patterns of FSS elements for good EM wave penetration through them were used, by etching the metal surfaces to form the desired slot shapes. Their occupying areas are relatively small compared to the rest

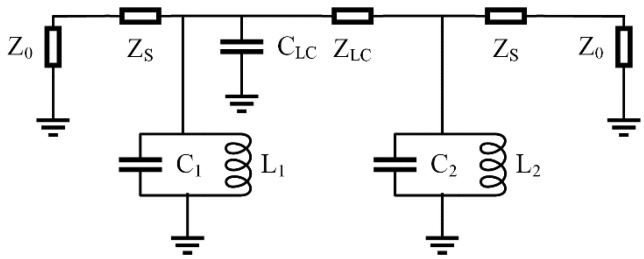

Fig. 2. EC of the LC-FSS. ($L_1 = 0.189$ nH, $L_2 = 0.197$ nH, $C_1 = 0.07$ pF, $C_2 = 0.053$ pF, $C_{\mathrm{LC}} = 0.1$ pF/0.125 pF).

of the metal surfaces for applying bias voltages. The areas of the metal surfaces are sufficient for the bias voltages to alter the global dielectric permittivity of the LC materials. The advantage of the slot-type elements is that they can be easily expanded in various dimensions without taking too much space. An efficient electric field distribution for the LC layer can be well generated by feeding a single bias voltage.

In practical design, the initial geometric parameters of the proposed LC-FSS, as illustrated in Fig. 1, were theoretically determined directly according to the coupled filter theory [1], [2], [21], [22] (i.e., the L on the top layer and the sum of A, B, C, and D on the bottom layer), which are afterward optimized by numerical full-wave simulations. The final parameters for fabrication were obtained from repeated optimization results by full-wave EM simulations using high-frequency structure simulator (HFSS) from Ansys [34]. This is the most straightforward way to achieve the desired results in FSS design [35]. The values of the unit cell's geometric parameters on the metallic layers, marked in Fig. 1(b) and (c), are given as follows: $Dx = Dy = 2.4$ mm, $W = 0.5$ mm, $L = 1.8$ mm, $g = 0.1$ mm, $A = 0.7$ mm, $B = 0.7$ mm, $C = 0.8$ mm, and $D = 0.3$ mm. It is noted that the proposed design can be applied to treat different polarization properties due to the symmetric patterns used on each metallic layer. However, in the current application, only the TE or TM polarization states of the incident plane wave, which are parallel to the rubbing direction of the LC layer in Fig. 1(a), are efficiently worked due to the inherent polarization sensitivity property of the LC materials. Therefore, in this research, the TE mode polarization wave, parallel to the rubbing direction of the fabricated LC-FSS prototype, was investigated for the representative performance illustration.

A simplified equivalent circuit (EC) model that has also used to verify the proposed LC-FSS is shown in Fig. 2, where the left and right branches represent the top and bottom metallic layers in Fig. 1, respectively. All lumped elements in this model were assumed to be ideal and the mutual inductive was also ignored due to the small influence. Since the metallic strips will bring the inductive (L) and the gaps between metals will generate capacitance (C), the top and bottom metallic layers can be converted into two parallel LC resonant circuits. The inductances L_1 and L_2 are mainly generated by the length Dx and the width of the strip. The capacitances C_1 and C_2 are determined by Jerusalem cross aperture gap (W) on top metallic layer and the size of the four slots on bottom metallic layer,

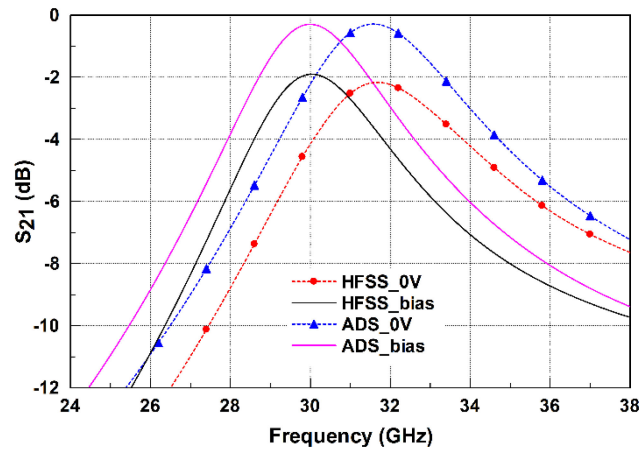

Fig. 3. Comparison of full-wave and EC.

respectively. The tunable middle layer (LC layer in Fig. 1) can be represented by the capacitance C_{LC}. The initial parameters of the EC model were determined by the formulas from the literature [36]–[38], which is the conventional approach used in FSS design. For example, (23-24) in [36] are the most used ones, which can compute the initial values of the inductive (L) and capacitance (C) [38]. Moreover, a curve-fitting approach has been applied to determine the model's final parameters, which is the most straightforward way to get the result without complicated calculations during the optimal design of FSS. These final parameters are shown in Fig. 2, where the capacitance C_{LC} can be switched from 0.1 to 0.125 pF to represent the LC-FSS without/with a bias voltage. The impedance Z_0 in air is about 377 Ω and the impedance in dielectric is calculated as $Z_0 = \sqrt{\varepsilon_r}$, Z_{S} is about 197.06 Ω and Z_{LC} is 228.59 Ω. The advanced design system (ADS) [39], which was widely used in the performance evaluation of analog circuit design, was used to simulate the EC model. The simulation results in comparison with the full-wave simulations by Ansys HFSS are illustrated in Fig. 3. Since no loss has been considered in the circuit model, a shift in insertion loss has been observed between the full-wave and circuit model simulations. Besides, the comparison results have shown a good agreement.

III. Performance Simulation

The numerical performance evaluations of the proposed LC-FSS were simulated by Ansys HFSS and are illustrated in Figs. 4–9. The reflection coefficients in Fig. 4 show two resonances at 30 and 31.6 GHz, respectively, for the bias voltages of 10 and 0 V. It implies that the resonant frequencies can be shifted from 31.6 to 30 GHz by altering the bias voltage. The transmission coefficients are roughly −2 dB, indicating a power loss of 2 dB. Note that the input of bias voltages results in low resonance frequencies, indicating an increase of dielectric constants by this LC material. Considering the −10 dB reflection coefficients as a threshold to determine the bandwidth, the bandwidth is observed by 29.3–32.3 GHz. In this case, one needs to use two bias voltages to achieve the frequency operation within this band. The

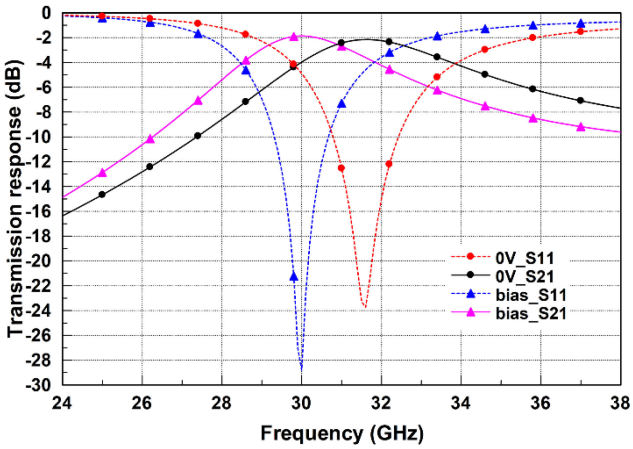

Fig. 4. Transmission and reflection responses for normally incident plane wave illumination with/without a bias voltage.

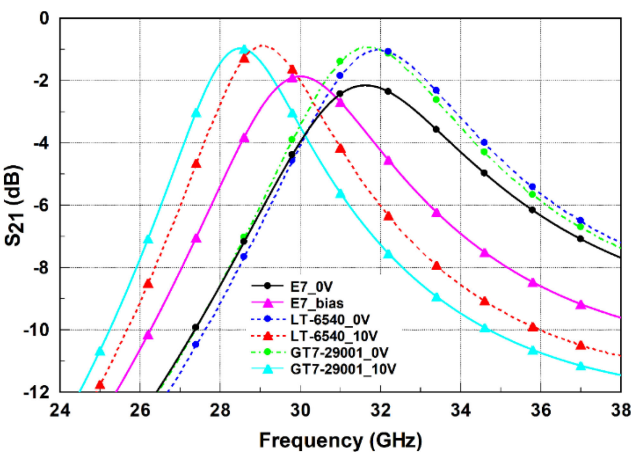

Fig. 5. Comparisons of transmission responses for normally incident plane wave illumination using different LC material with/without a bias voltage.

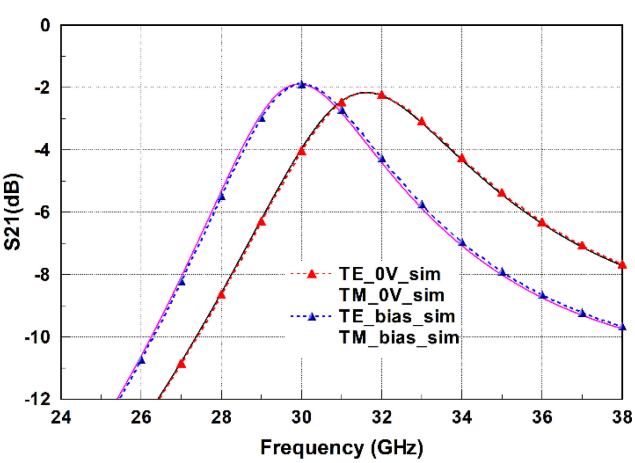

Fig. 6. Comparison of TE and TM polarization for normally incident plane wave illumination with/without a bias voltage.

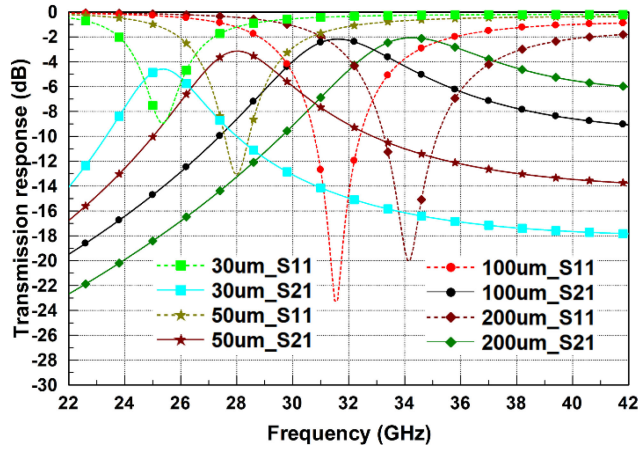

Fig. 7. Comparisons of transmission and reflection responses for normally incident plane wave illumination using different thickness of LC layer without a bias voltage.

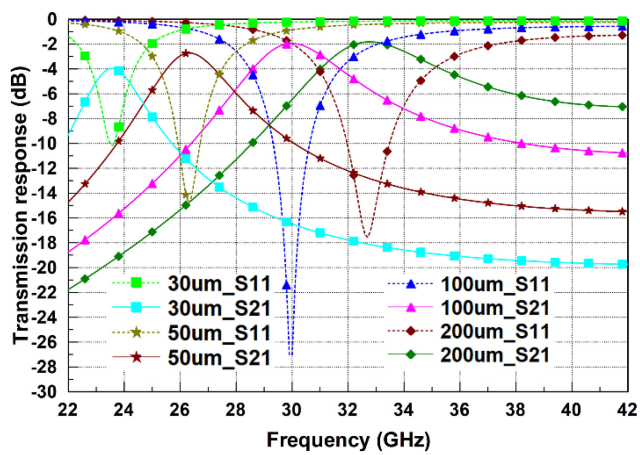

Fig. 8. Comparisons of transmission and reflection responses for normally incident plane wave illumination using different thickness of LC layer with a bias voltage.

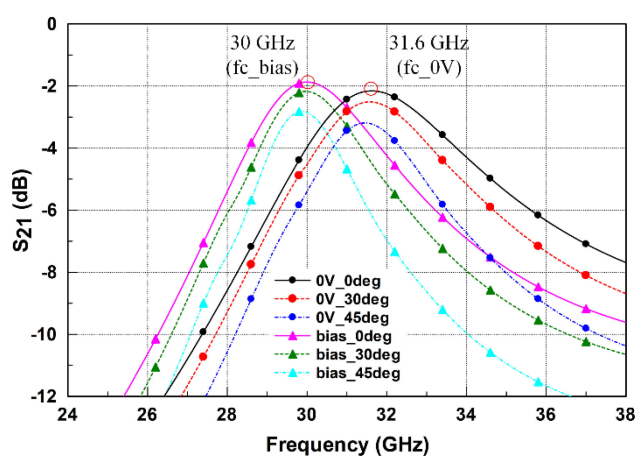

Fig. 9. Transmission responses for different incident angles.

dielectric constants of the LC materials have been changed from a vertical state (2.72) to a horizontal state (3.17). The tunable range of center frequencies is about 5.06%, deviation from the ordinary case of 31.6 GHz without applying any voltage.

Comparisons of transmission responses with other customized LC materials from the literatures have also been evaluated. The results, as shown in Fig. 5, indicate that both GT7-29001 and LT-6540 customized LC materials [18], [40] have a better performance than Merck-E7 LC material in the proposed work either in the frequency tunability or the insertion loss. The reasons are that both GT7-29001 and LT-6540 LC materials all have a dielectric tunability of nearly 1, which is double of the Merck-E7 LC material (0.45). Besides, the values of the loss tangent parameter for both GT7-29001 and LT-6540 LC materials are also much lower than the Merck-E7 LC material, which will result in a lower insertion loss. Nevertheless, both GT7-29001 and LT-6540 are still customized LC materials and have not yet been commercially available. Therefore, Merck-E7 LC material, which has been widely used for mass production in display applications, was used for experimental evaluation in the proposed work. However, the performance of the proposed work can be further raised by using either GT7-29001 or LT-6540 customized LC materials according to the simulation results.

Although the TE mode polarization wave was investigated for the representative performance illustration due to the inherent polarization sensitivity property of the LC materials, the transmission properties in terms of S-parameter for both TE and TM polarization waves, as shown in Fig. 6, have further verified that the proposed work can be applied to treat different polarization properties. Comparisons of transmission and reflection responses for normally incident plane wave illumination using different thickness of LC layer with/without a bias voltage are shown in Figs. 7 and 8, respectively. It shows that a thinner thickness of the LC layer has a narrower bandwidth but simultaneously will result in a higher insertion loss. Therefore, the thickness of 100 μm for the LC layer is chosen to validate its angle stability. Fig. 9 shows the transmission coefficient variations to incident angles of plane wave illuminations at 0°–45°. It is seen that the oblique incident angles do not alter the resonances. It simply increases the transmission losses. The losses are smaller than 1 dB compared to the normal incident case. It is also observed that applying the bias voltage also reduces the dielectric loss by almost 0.3 dB.

IV. Experimental Measurement and Evaluation

To verify the simulation performance of the proposed work, an LC-FSS prototype, as illustrated in Fig. 10, has been fabricated for experimental performance evaluation. The left-hand side of the prototypes shows the decomposed parts, which are two periodically patterned metallic layers. The trimmed corners on the two metallic layers are also seen for easy voltage input. These two corners are on the same sides when the two FSS metallic layers are oriented on the same face upward. In forming the integrated LC-FSS prototype, one of the two FSS metallic layers is flipped over and placed on top of each other. In this case, the two trimmed corners of the top and bottom FSS metallic layers

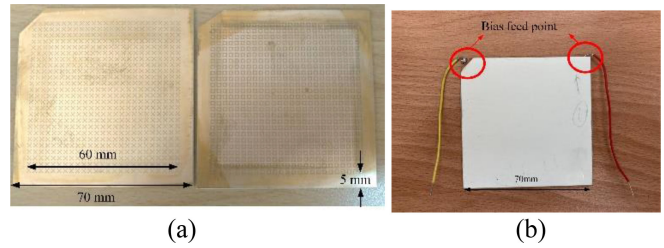

Fig. 10. Fabricated LC-FSS (a) alignment layers on top and bottom metallic layers and (b) prototype.

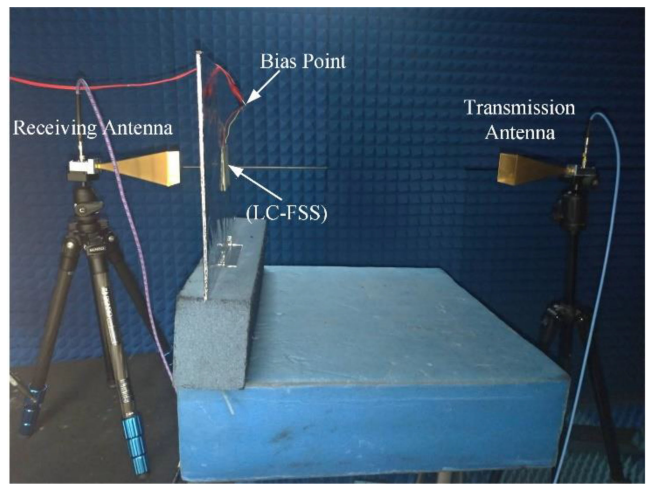

Fig. 11. Setup of experimental measurements.

are placed on the two adjacent corners of the integrated LC-FSS prototype. The bias voltages are applied to these two corners to different FSS metallic faces, as shown by the two wires on the top edge of the right-hand side prototype photo. Each FSS metallic layer implemented in this prototype consists of 25 × 25 unit cells on a physical area of 7 × 7 cm. These metallic layers also served as the host substrates of the alignment layers to realize the reconfigurability of the LC molecules. This was implemented by coating a PVA film on each metallic layer and then curing and rubbing. The rubbing direction parallel to the TE mode polarization wave was chosen during the fabrication. A pretilt angle of about 2° was induced from the rubbing process to orient the LC molecules between the two alignment layers. In comparison with the conventional optical fabrication process based on the glass substrates, the proposed work using PCB as the substrates is a low-cost approach but it is more challenging since the PCB deforming from heating during the fabrication of the alignment layer is very easy and will result in performance deviations.

In the measurements, the fabricated LC-FSS prototype was fixed on a holder by acrylic. To reduce the diffraction effects from the finite LC-FSS edges, this prototype was embedded into a rectangle of aluminum foil to prevent energy leakage from the truncations. This embedment has been proved in the literature [41] to be effective in increasing measurement reliability. The setup of the measurements is shown in Fig. 11, where a Keysight

TABLE I
COMPARISON OF LC-FSS WITH PREVIOUS WORKS

Paper	Unit cell size (mm)	Sample thickness (mm)	Frequency (GHz)	LC Permittivity Range ($\varepsilon_\perp - \varepsilon_\parallel$, $\Delta\varepsilon$)	LC loss tangent ($\tan\delta_\perp - \tan\delta_\parallel$)	Insertion loss (dB)	Tunability
[13]	~ 3.4×2.25	~1 mm	129.3 – 134	2.84 – 3.22, 0.38	0.01 – 0.02	3.7–10.4	3%(meas.)
[18]	~ 2×2	~5.4 mm	11.56 – 12.58	2.4 – 3.3, 0.9	0.0143 – 0.005	1.65–2.16	8.5% (sim.)
[42]	~ 7×7	~ 0.6 mm	8.98 – 9.49	2.5 – 3.3, 0.8	0.0143 – 0.0038	n/a	5.6% (sim.)
This work	2.4×2.4	~1.7 mm	28.58 – 30.04	2.72 – 3.17, 0.45	0.05 – 0.033	2.09–2.1	5.06%(sim.) 4.8%(meas.)

N5227A PNA network analyzer and two horn antennas were used to measure the transmission coefficients in a chamber, which can reduce the external interferences and antenna reflections during the measurements. The maximum physical size of the LC-FSS prototype that we can make is limited by the rubbing machine that we can use, which has a size limitation of less than 9 × 9 cm. Therefore, only the cases of normal incidence by the two horns' radiations are examined because of the LC-FSS size limitation. Oblique incidence illumination might cause oversized illuminating spots outside the LC-FSS prototype. Harmonic signals at various mmWave frequencies between 24–38 GHz fed the transmitting horn antenna. It is placed at about 0.6 m from the LC-FSS prototype to produce an approximate plane wave normally incident to the LC-FSS prototype. On the other hand, the receiving horn antenna was placed at about 0.2 m from the LC-FSS prototype. The varied distance between the transmitting and receiving horn antennas was used better to reduce the truncation diffractions from the limited LC-FSS prototype. A shorter distance between the LC-FSS prototype and the receiving horn antenna can avoid the illuminations from the transmitting horn antenna and reduce the truncation diffractions from the limited LC-FSS prototype. A Keysight arbitrary waveform generator (33 621 A) provides a low-frequency ac bias voltage (10 V) to the LC-FSS by the wires welding on the two metallic layers. The advantage of ac bias voltage compared to the dc bias is that it will not slow down the reaction speed of the LC molecules. Moreover, the impact of the applied ac voltage does not change with its frequency since only a few kilohertz (i.e., 1 kHz) was used.

The measured transmission responses of the LC-FSS prototype at normal incidence compared to the simulation results are shown in Fig. 12. The measurement results have shown that the resonant frequency can be shifted from 30.04 to 28.58 GHz when the bias voltage is applied. The frequency tunability is about 4.86%. Moreover, the maximum frequency deviations were only 4.73% and 4.94% with/without a bias voltage. These frequency deviations might result from the fabrication tolerance due to the deforming of the PCBs since, in the implementation of the alignment layers, high-temperature heating was required for each PCB to form a PVA film. Moreover, the relative permittivity used in the simulations was adopted from the literature [23], which might not match the correct values at Ka-band exactly. Although some frequency deviations existed from these comparisons, the measurement results agreed well with the simulations and validated the results.

Table I summarizes the comparisons with previous related works in [13], [18], and [42]. It is seen that the proposed

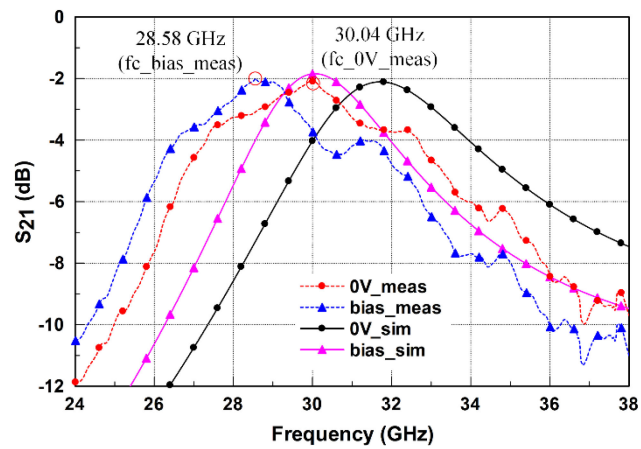

Fig. 12. Comparison of simulation and measurement results.

work has better performance. Compared to the work in [13] at 130 GHz, the developed LC-FSS at 30 GHz has a larger bandwidth by more than 60%. The transmission loss is also much smaller while the range of dielectric constant variation is also larger. Compared to the low-frequency case in [18], the dielectric tunability of the LC materials used is smaller by only close to 0.45, but the loss is similar. Note that the loss tangents of the previous work in [18] are 0.005 and 0.0143, much smaller than the used one in the proposed work. Besides, the thickness of the previous work in [18] is also beyond 5 mm, much thicker than the proposed work, which might restrict the practical applications. Compared to the simulation case in [42], the range of dielectric constant variation of the used LC material in the proposed work is much smaller, but the tunability is similar. Although the tunability of the proposed work is around 5% at the current stage, its performance can be further raised to around 10% by using either GT7-29001 or LT-6540 LC customized materials according to the previous simulation results. Furthermore, it can be used for a variety of applications, since most of these applications are relied not so much on frequency tunability, but more on other physical characteristics, such as spatial domain, time domain, and frequency domain conversions. For examples, it can be applied to dynamically change the transmission and reflection coefficients' characteristics of EM waves incident to the LC-FSS. The change of transmission characteristics helps to improve the characteristics of antenna operation, and the change of reflective characteristics can help the radar signal characteristics change, such as achieving the effect of invisibility and bullying. When it is used to produce continuous reflection

coefficient changes, which enables LC-FSS time domain and frequency domain characteristics to reduce spillover effects during conversion, thus improving system efficiency. Moreover, it can also integrate with the appropriate radar and communication to create new application functionalities.

V. Conclusion

In this research, an experimental investigation of a reconfigurable bandpass LC-FSS, which resonates at Ka-band frequencies, is reported. The low-cost Merck-E7 LC material with a dielectric constant tunable range of nearly 0.45, conventionally used for display applications, was employed to explore the frequency tunability at Ka-band. The simulation design has been further verified through experimental measurements, and the results have shown a good agreement. Compared to the previous research based on the customized LC materials and high-cost fabrication processing using glass substrates, the proposed work is the first experimental investigation for an LC-FSS resonating at Ka-band frequencies based on low-cost Merck-E7 LC material and PCB technology to the best of our knowledge. It will offer competitive performance and provides an alternative solution for mmWave applications at Ka-band.

Acknowledgment

The fruitful discussions during the LC-FSS prototype fabrication and measurement from Prof. C.-F. Yang (National Taiwan University of Science and Technology, Taiwan), Prof. H.-T. Chou (National Taiwan University, Taiwan), Prof. Tsung-Hsien Lin (National Sun Yat-sen University, Taiwan), Prof. Huang-Ming Chen (National Yang Ming Chiao Tung University, Taiwan), and Prof. Jia-De Lin (National Dong Hwa University, Taiwan) are much appreciated. Acknowledgments also go to Merck KGaA (Darmstadt, Germany) for partly financial and LC materials support.

References

[1] B. A. Munk, *Frequency Selective Surfaces: Theory and Design*, 1st ed. New York, NY, USA: Wiley, 2000.

[2] R. Mittra, C. H. Chan, and T. Cwik, "Techniques for analyzing frequency selective surfaces—A review," *Proc. IEEE*, vol. 76, no. 12, pp. 1593–1615, Dec. 1988, doi: 10.1109/5.16352.

[3] R. Dickie, R. Cahill, V. Fusco, H. S. Gamble, and N. Mitchell, "THz frequency selective surface filters for earth observation remote sensing instruments," *IEEE Trans. Terahertz Sci. Technol.*, vol. 1, no. 2, pp. 450–461, Nov. 2011, doi: 10.1109/TTHZ.2011.2129470.

[4] X. Sheng, J. Ge, K. Han, and X.-C. Zhu, "Transmissive/reflective frequency selective surface for satellite applications," *IEEE Antennas Wireless Propag. Lett.*, vol. 17, no. 7, pp. 1136–1140, Jul. 2018, doi: 10.1109/LAWP.2018.2830408.

[5] S. Ghosh, S. Bhattacharyya, D. Chaurasiya, and K. V. Srivastava, "An ultrawideband ultrathin metamaterial absorber based on circular split rings," *IEEE Antennas Wireless Propag. Lett.*, vol. 14, pp. 1172–1175, 2015, doi: 10.1109/LAWP.2015.2396302.

[6] A. Chatterjee and S. K. Parui, "Performance enhancement of a dual-band monopole antenna by using a frequency-selective surface-based corner reflector," *IEEE Trans. Antennas Propag.*, vol. 64, no. 6, pp. 2165–2171, Jun. 2016, doi: 10.1109/TAP.2016.2552543.

[7] L. Ji, Z. Zhang, and N. Liu, "A two-dimensional beam-steering partially reflective surface (PRS) antenna using a reconfigurable FSS structure," *IEEE Antennas Wireless Propag. Lett.*, vol. 18, no. 6, pp. 1076–1080, Jun. 2019, doi: 10.1109/LAWP.2019.2907641.

[8] K. D. Stephan, F. H. Spooner, and P. F. Goldsmith, "Quasioptical millimeter-wave hybrid and monolithic PIN diode switches," *IEEE Trans. Microw. Theory Techn.*, vol. 41, no. 10, pp. 1791–1798, Oct. 1993, doi: 10.1109/22.247925.

[9] A. Ebrahimi, Z. Shen, W. Withayachumnankul, S. F. Al-Sarawi, and D. Abbott, "Varactor-tunable second-order bandpass frequency-selective surface with embedded bias network," *IEEE Trans. Antennas Propag.*, vol. 64, no. 5, pp. 1672–1680, May 2016, doi: 10.1109/TAP.2016.2537378.

[10] J. M. Zendejas, J. P. Gianvittorio, Y. Rahmat-Samii, and J. W. Judy, "Magnetic MEMS reconfigurable frequency-selective surfaces," *J. Microelectromech. Syst.*, vol. 15, no. 3, pp. 613–623, Jun. 2006, doi: 10.1109/JMEMS.2005.863704.

[11] S. K. Ghosh, S. Das, and S. Bhattacharyya, "Graphene-based metasurface for tunable absorption and transmission characteristics in the near mid-infrared region," *IEEE Trans. Antennas Propag.*, vol. 70, no. 6, pp. 4600–4612, Jun. 2022, doi: 10.1109/TAP.2022.3140904.

[12] J. Shabanpour, S. Beyraghi, and A. Cheldavi, "Ultrafast reprogrammable multifunctional vanadium-dioxide-assisted metasurface for dynamic THz wavefront engineering," *Sci. Rep.*, vol. 10, 2020, Art. no. 8950, doi: 10.1038/s41598-020-65533-9.

[13] W. Hu et al., "Liquid crystal tunable mm wave frequency selective surface," *IEEE Microw. Wireless Compon. Lett.*, vol. 17, no. 9, pp. 667–669, Sep. 2007, doi: 10.1109/LMWC.2007.903455.

[14] R. Dickie, R. Cahill, V. Fusco, H. S. Gamble, and N. Mitchell, "THz frequency selective surface filters for earth observation remote sensing instruments," *IEEE Trans. Terahertz Sci. Technol.*, vol. 1, no. 2, pp. 450–461, Nov. 2011, doi: 10.1109/TTHZ.2011.2129470.

[15] R. Wang and L. Cai, "Liquid crystal based reconfigurable frequency selective surface for ISM applications," in *Proc. 9th Asia-Pacific Conf. Antennas Propag.*, 2020, pp. 1–2, doi: 10.1109/APCAP50217.2020.9246124.

[16] G. Yang, W. Kong, M. Chang, X. Liu, and Q. Wu, "Wideband tuning range frequency selective surface based on liquid crystal and tunable ability analysis," in *Proc. IEEE Conf. Electromagn. Field Comput.*, 2016, p. 1, doi: 10.1109/CEFC.2016.7816174.

[17] A. Ebrahimi, P. Yaghmaee, W. Withayachumnankul, C. Fumeaux, S. Al-Sarawi, and D. Abbott, "Interlayer tuning of X-band frequency-selective surface using liquid crystal," in *Proc. Asia-Pacific Microw. Conf. Proc.*, 2013, pp. 1118–1120, doi: 10.1109/APMC.2013.6695040.

[18] J.-F. Lv et al., "Tunable liquid crystal frequency selective surface with the compact unit cell, large tuning range, and the passband of flat-top and sharp roll-off," *J. Phys. D: Appl. Phys.*, vol. 54, no. 31, 2021, Art. no. 315001.

[19] G.-J. Ke, H.-H. Chou, G.-S. Lin, and C.-C. Lin, "Simulation design of LC-based tunable frequency selective surface at Ka-band," in *Proc. Opto-Electron. Commun. Conf.*, 2020, pp. 1–3, doi: 10.1109/OECC48412.2020.9273603.

[20] C.-C. Lin, G.-S. Lin, G.-J. Ke, and H.-H. Chou, "Tunable frequency selective surface (FSS) based on LC material for mmWave communications," in *Proc. Int. Symp. Antennas Propag.*, 2021, pp. 1–2, doi: 10.23919/ISAP47258.2021.9614366.

[21] J. S. G. Hong and M. J. Lancaster, *Microstrip Filters for RF/Microwave Applications*. New York, NY, USA: Wiley, 2004.

[22] D. S. Wang, P. Zhao, and C. H. Chan, "Design and analysis of a high-selectivity frequency-selective surface at 60 GHz," *IEEE Trans. Microw. Theory Techn.*, vol. 64, no. 6, pp. 1694–1703, Jun. 2016, doi: 10.1109/TMTT.2016.2557325.

[23] A. C. Polycarpou, M. A. Christou, and N. C. Papanicolaou, "Tunable patch antenna printed on a biased nematic liquid crystal cell," *IEEE Trans. Antennas Propag.*, vol. 62, no. 10, pp. 4980–4987, Oct. 2014, doi: 10.1109/TAP.2014.2344099.

[24] Y. Shang, Z. Shen, and S. Xiao, "On the design of single-layer circuit analog absorber using double-square-loop array," *IEEE Trans. Antennas Propag.*, vol. 61, no. 12, pp. 6022–6029, Dec. 2013, doi: 10.1109/TAP.2013.2280836.

[25] F. Costa, A. Monorchio, and G. Manara, "Analysis and design of ultra thin electromagnetic absorbers comprising resistively loaded high impedance surfaces," *IEEE Trans. Antennas Propag.*, vol. 58, no. 5, pp. 1551–1558, May 2010, doi: 10.1109/TAP.2010.2044329.

[26] S. Ghosh, S. Bhattacharyya, D. Chaurasiya, and K. V. Srivastava, "Polarization-insensitive and wide-angle multi-layer metamaterial absorber with variable bandwidths," *Electron. Lett.*, vol. 51, no. 14, pp. 1050–1052, Jul. 2015.

[27] S. Ghosh and K. V. Srivastava, "A dual-band tunable frequency selective surface with independent wideband tuning," *IEEE Antennas Wireless Propag. Lett.*, vol. 19, no. 10, pp. 1808–1812, Oct. 2020, doi: 10.1109/LAWP.2020.3019584.

[28] S. Ghosh and K. V. Srivastava, "Broadband polarization-insensitive tunable frequency selective surface for wideband shielding," *IEEE Trans. Electromagn. Compat.*, vol. 60, no. 1, pp. 166–172, Feb. 2018, doi: 10.1109/TEMC.2017.2706359.

[29] S. Ghosh and K. V. Srivastava, "A polarization-independent broadband multilayer switchable absorber using active frequency selective surface," *IEEE Antennas Wireless Propag. Lett.*, vol. 16, pp. 3147–3150, 2017, doi: 10.1109/LAWP.2017.2766100.

[30] P. Kong, X. W. Yu, M. Y. Zhao, Y. He, L. Miao, and J. J. Jiang, "Switchable frequency selective surfaces absorber/reflector for wideband applications," *J. Electromagn. Waves Appl.*, vol. 29, no. 11, pp. 1473–1485, 2015, doi: 10.1080/09205071.2015.1049713.

[31] Q. Zhang, Z. Shen, J. Wang, and K. S. Lee, "Design of a switchable microwave absorber," *IEEE Antennas Wireless Propag. Lett.*, vol. 11, pp. 1158–1161, 2012, doi: 10.1109/LAWP.2012.2220115.

[32] Rogers Corporation, "RO4000 series high frequency circuit materials," RO4350B datasheet, 2018.

[33] K. Sarabandi and N. Behdad, "A frequency selective surface with miniaturized elements," *IEEE Trans. Antennas Propag.*, vol. 55, no. 5, pp. 1239–1245, May 2007, doi: 10.1109/TAP.2007.895567.

[34] Ansys HFSS: High Frequency Electromagnetic Field Simulation Software, 2020. Accessed: May 22, 2020. [Online]. Available:https://www.ansys.com/zh-tw/products/electronics/ansys-hfss

[35] H.-H. Chou and G.-J. Ke, "Narrow bandpass frequency selective surface with high level of angular stability at Ka-band," *IEEE Microw. Wireless Compon. Lett.*, vol. 31, no. 4, pp. 361–364, Apr. 2021, doi: 10.1109/LMWC.2021.3054016.

[36] M. A. Al-Joumayly and N. Behdad, "A generalized method for synthesizing low-profile, band-pass frequency selective surfaces with non-resonant constituting elements," *IEEE Trans. Antennas Propag.*, vol. 58, no. 12, pp. 4033–4041, Dec. 2010, doi: 10.1109/TAP.2010.2078474.

[37] F. Costa, A. Monorchio, and G. Manara, "Efficient analysis of frequency-selective surfaces by a simple equivalent-circuit model," *IEEE Antennas Propag. Mag.*, vol. 54, no. 4, pp. 35–48, Aug. 2012, doi: 10.1109/MAP.2012.6309153.

[38] O. Luukkonen et al., "Simple and accurate analytical model of planar grids and high-impedance surfaces comprising metal strips or patches," *IEEE Trans. Antennas Propag.*, vol. 56, no. 6, pp. 1624–1632, Jun. 2008, doi: 10.1109/TAP.2008.923327.

[39] Keysight Technologies ADS: Advanced design system, 2021. Accessed: Jun. 6, 2021. [Online]. Available: https://www.keysight.com/us/en/products/software/pathwave-design-software/pathwave-advanced-designsystem.html

[40] C. Fritzsch, B. Snow, J. Sargent, D. Klass, S. Kaur, and O. Parri, "Liquid crystals beyond displays: Smart antennas and digital optics," SID Symp. Dig. Tech. Papers, 2019.

[41] M. Al-Joumayly and N. Behdad, "A new technique for design of low-profile, second-order, bandpass frequency selective surfaces," *IEEE Trans. Antennas Propag.*, vol. 57, no. 2, pp. 452–459, Feb. 2009, doi: 10.1109/TAP.2008.2011382.

[42] A. Ebrahimi, P. Yaghmaee, W. Withayachumnankul, C. Fumeaux, S. Al-Sarawi, and D. Abbott, "Interlayer tuning of X-band frequency-selective surface using liquid crystal," in *Proc. Asia-Pacific Microw. Conf.*, 2013, pp. 1118–1120, doi: 10.1109/APMC.2013.6695040.

Hsi-Hsir Chou (Senior Member, IEEE) was born in Taiwan. He received the Ph.D. degree in engineering from Cambridge University, Cambridge, U.K., in 2008.

He joined the Department of Engineering Science, Oxford University, Oxford, U.K., in July 2008 as a Postdoctoral Researcher sponsored by Samsung Electronics Company Ltd., Suwon, South Korea. He has been with the Department of Electronic and Computer Engineering, National Taiwan University of Science and Technology, Taiwan, since 2013 and is currently an Associate Professor. His current research interests include free-space optical interconnection technologies, optical wireless communications, and liquid crystal devices for photonics and mmWave applications.

Dr. Chou is a lifetime member of Trinity College, Cambridge, U.K., and has been a Fellow of the Cambridge Overseas Society, Cambridge University, U.K., since 2005.

Guan-Jhou Ke was born in Changhua, Taiwan. He received the B.Sc. degree in electrical engineering from National Taiwan Ocean University, Keelung, Taiwan, in 2019, and the M.Sc. degree in electronic and computer engineering from National Taiwan University of Science and Technology (Taiwan Tech), Taipei, Taiwan, in 2021.

He is currently a Flash Engineer with Kingston Technology Corporation, Hsinchu, Taiwan. His current research interests include nonvolatile memory devices and signal integrity.

Cheng-Chung Lin was born in Chiayi, Taiwan, on December 1, 1971. He received the B.S. and M.S. degrees in earth science from National Cheng Kung University, Tainan, Taiwan, in 1995 and 1998, respectively, and the Ph.D. degree in space science from National Central University, Taoyuan, Taiwan, in 2006.

He joined National Chung-Shan Institute of Science and Technology, Taoyuan, Taiwan, in 2009 as a Researcher in development of techniques in radar cross-sectional measurement and in radar absorbing materials.

Guo-Sheng Lin was born in Tainan, Taiwan, in 1988. He received the Ph.D. degree in microelectronics from National Cheng Kung University, Tainan, Taiwan, in 2018.

He joined National Chung-Shan Institute of Science and Technology, Taoyuan, Taiwan, in 2018 as a Researcher in development of techniques in radar cross-sectional measurement and in radar absorbing materials.